

第二十一屆 旺宏科學獎

成果報告書

參賽編號： SA21-184

作品名稱： Antimicrobial Activity of Chemically Reduced Electrospun Polyacrylonitrile Silver Nanoparticle (PAN-AgNP) and Copper Nanoparticle (PAN-CuNP) Nanocomposites Against *E. coli* and *L. crispatus*

姓 名： William Bing-Sian Wang

關鍵字： Silver, Copper, Nanoparticles, Polyacrylonitrile (PAN), Electrospinning, *E. coli*, *L. crispatus*

Abstract

Microorganism induced diseases are easily transmitted in the air or via contact surfaces through respiratory droplets. It has become increasingly important for researchers to discover materials that can be implemented in in vitro surface contact settings and disrupt microorganism growth before transmission. Silver and copper are known to have antimicrobial properties and have been used in the past in medical applications. This study investigates the antibacterial properties of polyacrylonitrile (PAN) based nanofibers coated with different concentrations of silver or copper nanoparticles (AgNPs, CuNPs). Different concentrations of silver nitrate (AgNO_3) or copper sulfate (CuSO_4) were mixed with polyacrylonitrile (PAN) and *N,N*-Dimethylformamide (DMF) solution, a common electrospinning solvent that also acts as a reducing agent for AgNO_3 and CuSO_4 , in turn forming AgNPs and CuNPs during the reduction process. The resulting colloidal solutions were electrospun into nanofibers and characterized via various analysis techniques, including Atomic Force Microscopy (AFM), Scanning Electron Microscopy (SEM), Transmission Electron Microscopy (TEM), Dynamic Light Scattering (DLS), and X-Ray Photoelectron Spectroscopy (XPS). Cultures of *Escherichia coli* (*E. coli*) and *Lactobacillus crispatus* (*L. crispatus*) were incubated with cutouts of various nanocomposites using disk diffusion methods on nutrient medium agar, while Zone of Inhibition (ZOI) tests were conducted to quantify the polymers' antibacterial properties. Herein, we disclose that PAN-AgNP and PAN-CuNP nanofibers demonstrate antibacterial activity against bacteria. Moreover, both types of nanocomposites retain a certain degree of antimicrobial longevity; samples stored for approximately 90 days demonstrate similar antibacterial activity when compared to their newly electrospun counterparts. Our findings reveal that PAN-AgNP and PAN-CuNP nanofibers synthesized via chemical reduction and electrospinning methods have the potential to be used in high-contact surfaces at risk of contracting microbial infections, such as masks, pads, and surgical equipment.

Keywords: Silver; Copper; Nanoparticles; Polyacrylonitrile (PAN); Electrospinning; Nanofibers; *E.coli*; *L. crispatus*

Table of Contents

Abstract	1
Table of Contents	2
1. Introduction	3
1.1 Motivations	3
1.2 Project Purpose	3
2. Literature Review	4
3. Experimental Overview	6
4. Materials and Instruments	7
5. Procedures and Methods	8
5.1 Preparation of PAN/DMF/AgNP and PAN/DMF/CuNP Solutions	8
5.2 Electrospinning	8
5.3 PAN-AgNP Nanofiber and PAN-CuNP Nanofiber Characterization Techniques	9
5.4 Bacterial Culture Preparation and Serial Dilution	9
5.5 Zone of Inhibition Antibacterial Tests	10
6. Results	11
6.1 Morphology Analysis of Nanofibers with AFM	11
6.2 Elemental Analysis of PAN-AgNP and PAN-CuNP Nanofibers with SEM and EDX	12
6.3 Characterization of AgNPs and CuNPs Size with TEM and DLS	15
6.4 Comparison of Preserved and New PAN-AgNP and PAN-CuNP Nanocomposites	18
6.5 Antibacterial Efficiency Tests on <i>E. coli</i> and <i>L. crispatus</i>	18
7. Discussion	21
7.1 Colloidal Synthesis and Polymer Characterization	21
7.2 Evaluation of Nanocomposite Antibacterial Efficiency	22
8. Conclusions	23
9. Future Works	24
10. References	25
Appendix	A1

1. Introduction

1.1. Motivations

Infectious diseases are easily transmitted in the air or via contact surfaces through respiratory droplets expelled from a person's nose or mouth [1,2]. Recently, human beings have suffered from negative clinical outcomes due to the rapid transmission and high infectivity of these diseases; prominent examples of these diseases include Community Acquired Pneumonia (CAP) and the SARS-CoV-2 infection [2,3]. It has proven to be difficult for scientists to find appropriate drugs that can be used to efficiently treat and prevent these diseases. Hence, this project aims to evaluate the effectiveness of an alternative novel antimicrobial agent engineered using chemical reduction and electrospinning methods.

1.2. Project Purpose

In this project, we aim to analyze the characteristics of polyacrylonitrile-silver nanoparticle (PAN-AgNP) and polyacrylonitrile-copper nanoparticle (PAN-CuNP) nanofibers and their subsequent nanoparticles (NPs) after the nanocomposites have been synthesized via chemical reduction and electrospinning procedures. The nanocomposites will also be characterized with Atomic Force Microscopy (AFM), Scanning Electron Microscopy (SEM), Transmission Electron Microscopy (TEM), Dynamic Light Scattering (DLS) and X-ray photoelectron spectroscopy (XPS); these tests will allow us to expound upon and understand the properties of these nanocomposites.

Additionally, the antibacterial efficiency of PAN-AgNP and PAN-CuNP nanofibers will be analyzed. PAN-AgNP and PAN-CuNP nanofibers synthesized from different weight concentrations (wt.%) of AgNO₃ and CuSO₄ will be observed and compared for their differences in antibacterial activity on *Escherichia coli* (*E. coli*) and *Lactobacillus crispatus* (*L. crispatus*). PAN-AgNP and PAN-CuNP nanocomposites will be analyzed and measured for their antibacterial efficiency in Zone of Inhibition (ZOI) tests against *E. coli* and *L. crispatus*. *E. coli* is a gram-negative bacterium and *L. crispatus* is a gram-positive bacterium; as both bacteria species are ubiquitous in nature, these trials can also act as part of a preliminary test that provides insight towards the behavior of these nanocomposites on various pathogens.

The longevity of PAN-AgNP and PAN-CuNP nanocomposites will also be evaluated. These nanofibers will be stored under room temperature. After approximately 90 days of storage, the nanocomposites will be analyzed for their antibacterial efficiency via ZOI tests on *E. coli* and *L. crispatus*; their antibacterial activity will also be compared to newly electrospun fibers.

2. Literature Review

Metals such as silver (Ag) and copper (Cu) have been frequently used in the past as antimicrobial agents in medical and environmental science applications [4]. Silver has been used as a form of wound dressing for burns and microbial infections [5]. On the other hand, copper is an accessible and relatively cheaper material that is known to have antimicrobial properties. It is also a trace element in the human body and is non-toxic when consumed at low levels [6,7]. When synthesized into nanomaterials like silver or copper nanoparticles (AgNPs, CuNPs), silver and copper undergo significant physiochemical changes that allow them to have better permeability in pathogens than their bulk counterparts due to their size-dependent crystalline structure and high surface area-to-volume ratio [8].

As AgNPs and CuNPs come into contact with bacteria, they bind to their cell wall and cell membrane and begin inhibiting cellular respiration. Moreover, the corresponding positively charged silver and copper ions of the NPs rupture the negatively charged peptidoglycan-based bacteria cell wall via depolarization and releases the bacteria's internal cell contents [9,10]. During this process, reactive oxygen species (ROSs) are also created, in turn interrupting DNA replication [9,11]. Biochemical processes inside the cell are also disrupted as silver and copper ions interact with sulfur (S) containing biomolecules, replacing their respective H^+ groups and altering their molecular structure via denaturation [9,12]. The antibacterial properties of AgNPs and CuNPs ultimately result in the subsequent biochemical degradation and death of the targeted microorganism (**Figure 1**).

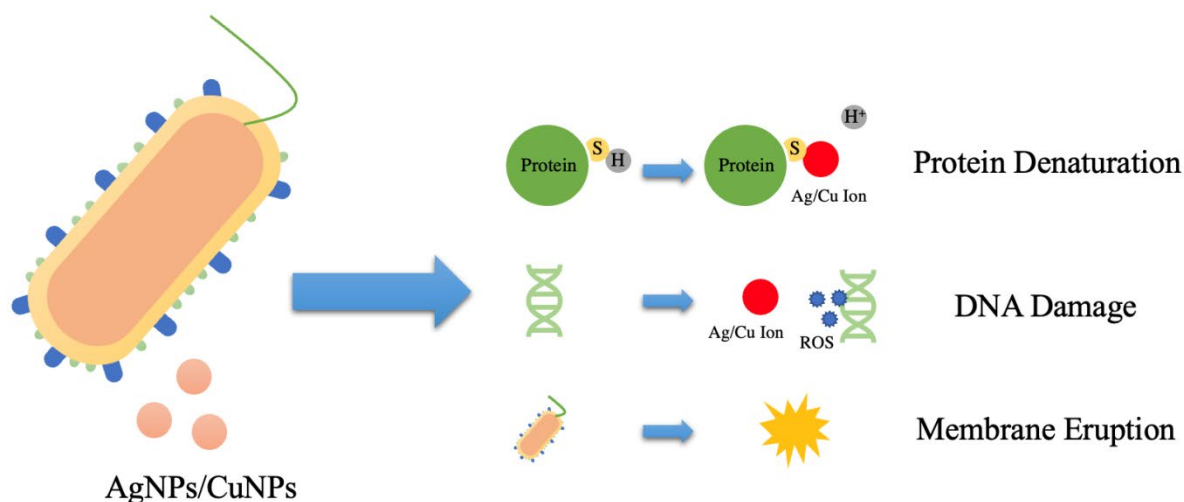


Figure 1. Schematic Diagram Demonstrating the Antibacterial Mechanism of AgNPs/CuNPs and Ag/Cu Ions, which Induces Protein, DNA, and Cell Membrane Damage in Bacteria Cells.

Carbon-based polymer nanofibers are commonly used in surface engineering applications due to their high surface area to volume ratio, malleability, and compact structure [13,14]. Among various organic carbon polymers, polyacrylonitrile (PAN) could be widely adopted for

antimicrobial nanocomposite engineering due to effective fibril formation via electrospinning [15,16]. PAN has unique thermal stability properties that allows it to degrade before reaching its melting point [17,18]. Moreover, PAN is known for its strong mechanical characteristics and high carbon yield, making it the ideal substance for building a long lasting, solvent resistant material [19].

The chemical formation of AgNPs and CuNPs and their synthesis with PAN can be initiated with *N,N*-Dimethylformamide (DMF). While DMF is a conventional organic chemistry solvent, it is a potent reducing agent that can reduce metal salts during colloidal solution formation due to its high oxidation potential (1.9 V vs Standard Hydrogen Electrode) [20]. This is because DMF contains a terminal carbonyl group that is oxidized to a carboxylic group while metal ions present in metal salts are reduced to atoms in the presence of water [21]. Moreover, DMF has a high dielectric constant, is an electrically conductive solvent, and has low vapor pressure [22]. Since metal nanoparticle containing carbon polymer nanofibers are usually synthesized with electrospinning techniques, DMF can also be used as an electrospinning solvent for PAN. DMF improves the crystallinity and decreases the diameter of electrospun fibers, further increasing the surface area-to-volume ratio for electrospun polymer nanocomposites [23]. Hence, PAN/DMF/AgNP or PAN/DMF/CuNP colloidal solutions could be spun into PAN-AgNP and PAN-CuNP filaments via the use of an electrospinner. The high voltage electric field gradient created by the electrospinner spins, solidifies, and coagulates the colloidal solution into a solid nanocomposite (**Figure 2**).

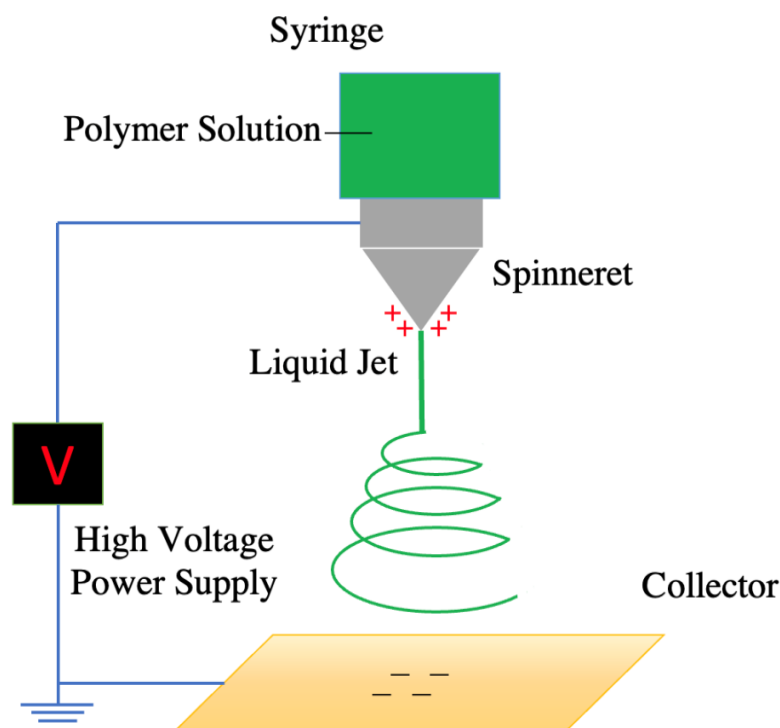
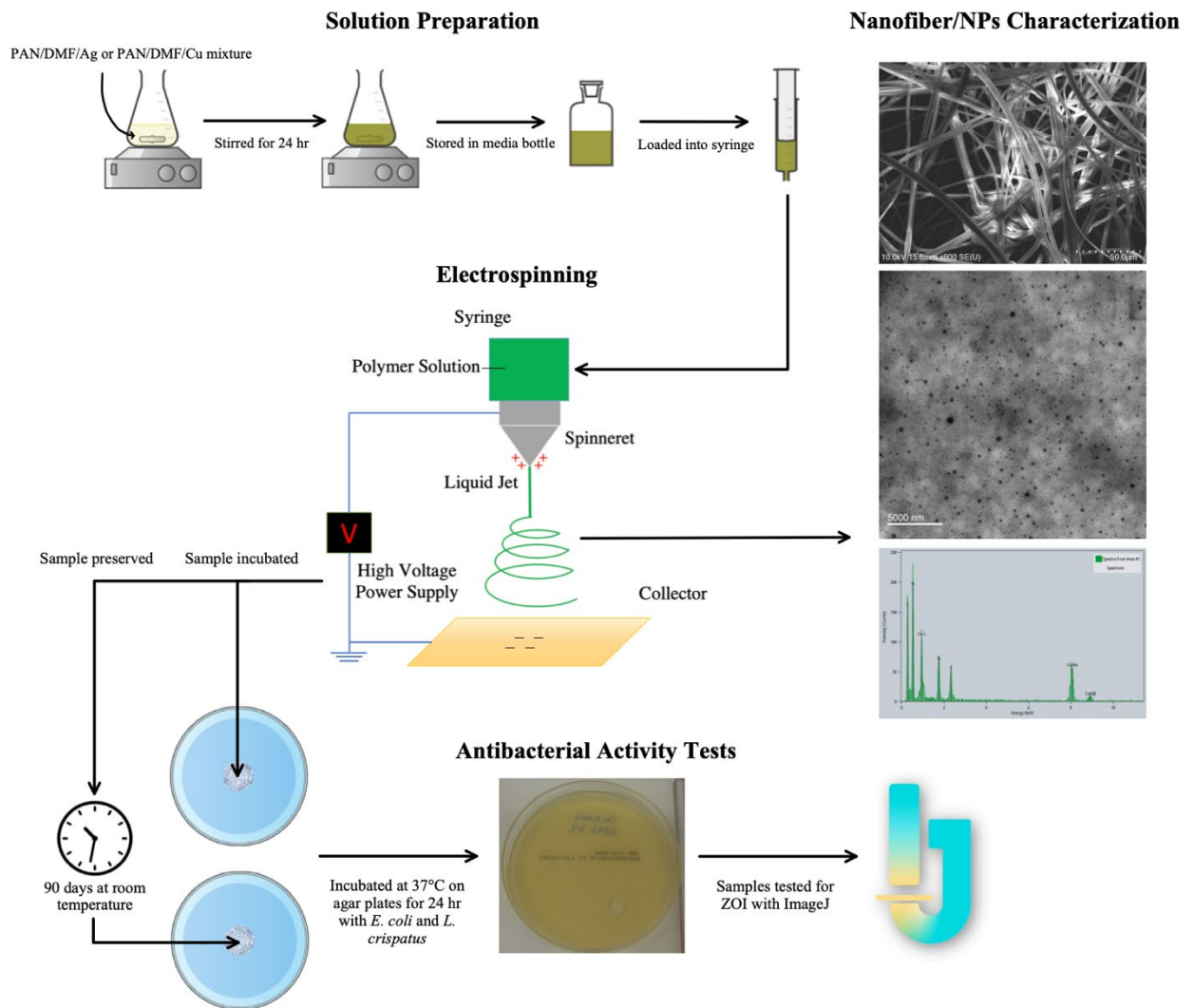


Figure 2. Schematic Diagram of Electrospinner Creating Carbon-Based Polymer Nanofibers.

3. Experimental Overview



4. Materials and Instruments

Material/Chemical	Provider/Manufacturer
Polyacrylonitrile (PAN _(s))	Merck Co. Ltd., Sigma-Aldrich Company, Neihu, Taipei, Taiwan
<i>N,N</i> -Dimethylformamide (DMF _(aq))	Merck Co. Ltd., Sigma-Aldrich Company, Neihu, Taipei, Taiwan
Silver Nitrate (AgNO _{3(s)})	Merck Co. Ltd., Sigma-Aldrich Company, Neihu, Taipei, Taiwan
Copper Sulfate (CuSO _{4(s)})	Merck Co. Ltd., Sigma-Aldrich Company, Neihu, Taipei, Taiwan
Silver Foil	Han Fu Tang Arts & Crafts Store, Kaohsiung, Taiwan
Copper Foil	Han Fu Tang Arts & Crafts Store, Kaohsiung, Taiwan
de Man, Rogosa and Sharpe (MRS) Broth Powder	Merck Co. Ltd., Sigma-Aldrich Company, Neihu, Taipei, Taiwan
Tryptic Soy Broth (TSB) Powder	Merck Co. Ltd., Sigma-Aldrich Company, Neihu, Taipei, Taiwan

Instrument	Provider/Manufacturer
Magnetic Stir Bar (15×8 mm)	Merck Co. Ltd., Sigma-Aldrich Company, Neihu, Taipei, Taiwan
Luer Slip Syringe	Terumo Co. Ltd., Shibuya City, Tokyo, Japan
Syringe Pump	Inovenso Co. Ltd., Istanbul, Turkey
Electrospinner	Inovenso Co. Ltd., Istanbul, Turkey
Hole Puncher (6.5 mm Diameter)	Long Jer Precise Industry Co. Ltd.
Shaking Incubator	Thermo Fisher Scientific, Waltham, Massachusetts, United States 127
Non-shaking Incubator	Deng Yng Co. Ltd., Taishan District, Taipei, Taiwan
UV-VIS Optical Density Spectrophotometer	Vernier Software Technology, Beaverton, Oregon, United States
Atomic Force Microscope (AFM), XE7	Park Systems, Suwon-si, South Korea
XEI Imaging Software	Park Systems, Suwon-si, South Korea
Scanning Electron Microscope (SEM), Phenom ProX G6 Desktop	Thermo Fisher Scientific, Waltham, Massachusetts, United States 127
Scanning Electron Microscope (SEM), SU8220	Hitachi High-Technologies Corporation, Tokyo, Japan
Transmission Electron Microscope (TEM), Talos F200X G2	Thermo Fisher Scientific, Waltham, Massachusetts, United States 127
Dynamic Light Scattering (DLS) N5 Submicrometer Particle Size Analyzer	Beckman Coulter, Inc., U.S.A.
ImageJ (Java-based image processing program)	Wayne Rasband, National Institutes of Health (NIH), Bethesda, Maryland, United States

Bacterial Strain	Provider
<i>Escherichia coli</i> (K-12 DH5α)	Bioresource Collection and Research Center, Hsinchu, Taiwan
<i>Lactobacillus crispatus</i> (14168)	Bioresource Collection and Research Center, Hsinchu, Taiwan

5. Procedures and Methods

5.1. Preparation of PAN/DMF/AgNP and PAN/DMF/CuNP Solutions

Prior to synthesizing AgNP-coated and CuNP-coated PAN nanofibers with an electrospinner, different colloidal electrospinning solutions were prepared. Seven distinct PAN solutions were prepared by dissolving 10 wt.% of PAN in 50 mL DMF. Different percentages (5%, 10%, and 15% wt.% w.r.t to weight of PAN) of AgNO₃ and CuSO₄ were simultaneously dissolved in six of the solutions. The seventh solution will be left as a pure PAN-based control that will not contain AgNPs or CuNPs (**Figure 3a**). The solutions were then stirred using a 50×8 mm magnetic stir bar at 200 rpm for 24 hours. After the chemicals have homogenized and completely dissolved, color changes could be observed in the colloidal solutions, in turn qualitatively screening for and signifying the formation of AgNPs and CuNPs in PAN/DMF solution (**Figure 3b**, **Figure 3c**). PAN/DMF/AgNP solutions of all concentrations must also be protected from light due to the light sensitivity and degradation of silver.



Figure 3a.
Pure PAN/DMF
Solution



Figure 3b.
15% PAN/DMF/AgNP
Solution



Figure 3c.
15% PAN/DMF/CuNP
Solution

5.2. Electrospinning

5 mL of PAN/DMF/AgNP or PAN/DMF/CuNP solution created from a specific concentration of AgNO₃ or CuSO₄ (0%, 5%, 10%, and 15% wt.% with respect to weight of PAN) was loaded into a 10 mL single use Luer Slip Syringe. The syringe was then affixed to a syringe pump and connected to an electrospinner via a single use plastic tube. A 200×200 mm² piece of aluminum foil was attached onto the movable collection platform of the electrospinner, which was locked in a position 100 mm away from the electrospinning nozzle. The negative electrode clip was then attached to the aluminum foil to allow for the creation of an electric field during the electrospinning process (**Figure 4**).

The electrospinner was set to operate at a voltage of 30 kV, and the injection rate was adjusted to 2.5 mL/hr. Electrospinning concluded once the precursor solution was completely used up and spun into PAN-AgNP or PAN-CuNP nanofibers (**Figure 5**).



Figure 4. Image of Electrospinner Creating Carbon-Based Polymer Nanofibers



Figure 5. PAN-CuNP Nanofibers Coated on Aluminum Foil

5.3. PAN-AgNP Nanofiber and PAN-CuNP Nanofiber Characterization Techniques

3D topographical images of the fibers were obtained by using a XE7 Atomic Force Microscope (AFM) to analyze the surface morphology of the fibers and the AgNPs/CuNPs coated on them. The AFM images were analyzed using the XEI imaging software, a Java-based image processing program exclusively designed for XE Atomic Force Microscopy.

A SU8220 Scanning Electron Microscope (SEM) was used in this study to determine fiber morphology and thickness. Energy Dispersive X-Ray (EDX) elemental analysis was also conducted in the SEM to analyze the elemental contents of the nanofibers.

The diameters of the AgNPs/CuNPs that were suspended in PAN/DMF/AgNP or PAN/DMF/CuNP solution were measured with length characterization tools with a Transmission Electron Microscope (TEM). In addition, Dynamic Light Scattering (DLS) was also used to determine the size distribution of AgNPs/CuNPs suspended in PAN-DMF solution.

5.4. Bacterial Culture Preparation and Serial Dilution

Bacteria media and growth plates were prepared prior to growing bacteria strains. 2.5% wt.% TSB powder and MRS broth powder were dissolved separately in distilled water and sterilized using an autoclave to create the growth media for the two bacteria cultures used in this study. Similarly, 2.5% wt.% TSB powder or MRS broth powder was dissolved in distilled water with 1.5% wt.% agar powder, sterilized in an autoclave, and evenly poured into 100×15 mm petri dishes. Nutrient plates were formed after the solution solidified in the petri dishes.

Cultures of *E. coli* were grown in 2.5% TSB and cultures *L. crispatus* were grown in 2.5% MRS broth in a shaking incubator set at 37 °C and 200 rpm for 24 hours. The cultures were then diluted to a 0.5 MacFarland bacterial turbidity standard with a UV-VIS optical density spectrophotometer, which provides an optical density comparable to the density of a bacterial suspension with a 1.5×10^8 colony forming units (CFU/ml). 50 μ L of *E. coli* and *L. crispatus* liquid culture were added to their corresponding nutrient agar plates, and glass beads were used to equally distribute the bacteria on the plate (**Figure 6**).

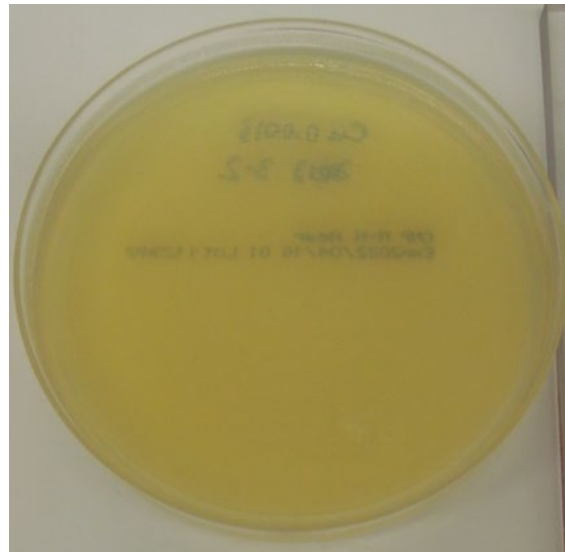


Figure 6. Image of Agar Plate with Evident Bacteria Growth

5.5. Zone of Inhibition Antibacterial Tests

A 6.5 mm diameter hole puncher was used to cut out all nanofiber and control disks (**Figure 7**). Disks of diameter 6.5 mm for each of the four concentrations (0%, 5%, 10%, and 15% wt.% w.r.t to weight of PAN) of PAN-AgNP and PAN-CuNP nanofibers were placed onto agar plates for both *E. coli* and *L. crispatus*. Pure silver and copper foil disks of the same diameter were also used in ZOI antibacterial tests under the same conditions for *E. coli* and *L. crispatus*.

Another distinct group of nanocomposites of the same aforementioned concentrations were preserved under room temperature for approximately 90 days. After approximately 90 days of preservation, they were also cut out into disks of diameter 6.5 mm and used in ZOI bacterial tests for *E. coli* and *L. crispatus*.

The plates were then incubated with the fiber disks at 37 °C for 24 hours in a non-shaking incubator. After incubation, the inhibition diameter of the various nanofiber and control disks were measured with ImageJ, a Java-based image processing program commonly used to analyze ZOI tests.

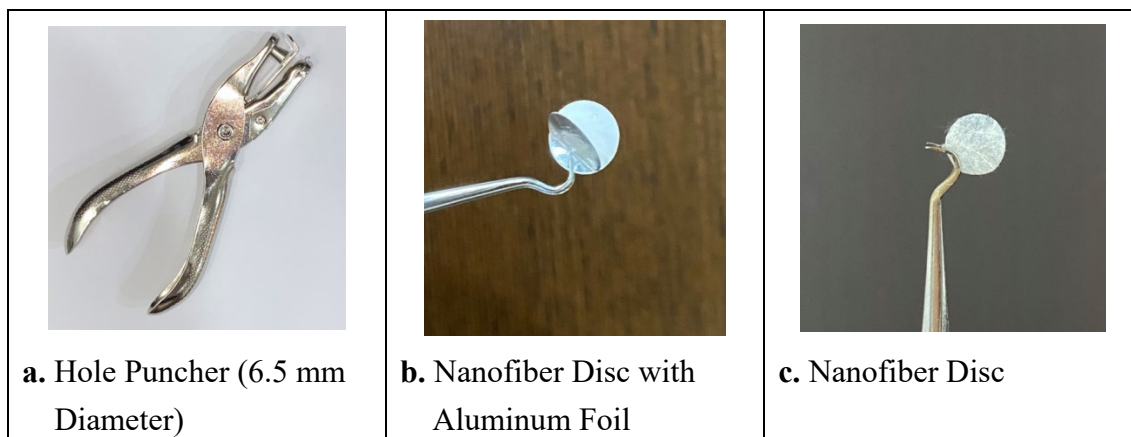


Figure 7. Hole Punching Apparatus and Products

6. Results

6.1. Morphology Analysis of Nanofibers with AFM

The AFM is a powerful non-optical imaging technique used for surface analysis. PAN nanofiber disks were analyzed using an AFM to determine their topographical structure. Images were obtained in a $2500 \mu\text{m}^2$ frame with a non-etching AFM cantilever at a scan rate of 0.5 Hz (**Figure 8**)

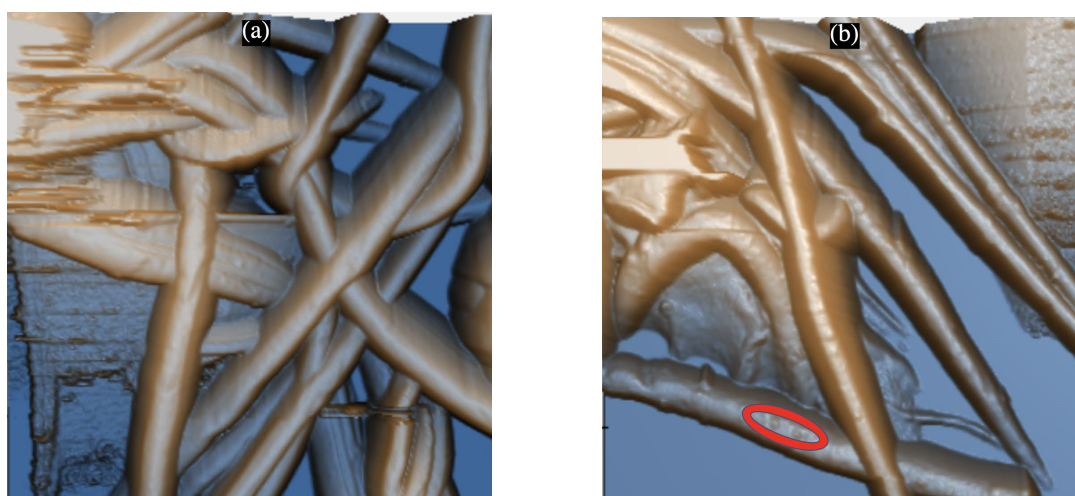


Figure 8. (a) 3D AFM Scanning Image of Pure PAN Nanofiber Disk (b) 3D AFM Scanning Image of 15% PAN-CuNP Nanofiber Disk, where Circled Portions Show Evidence of Nanoparticle Formation

PAN nanofibers were found to have a compact structure, as they scaffold atop each other and frequently intersect. As shown in **Figure 8a**, NPs were not visible on pure PAN nanofibers. On the other hand, the image verifies that the nanofibers were coated with NPs, as individual NPs can be observed as small bumps on the surface of a PAN nanofiber (**Figure 8b**).

6.2. Elemental Analysis of PAN-AgNP and PAN-CuNP Nanofibers with SEM and EDX

Pure PAN nanofibers were first analyzed with SEM techniques. As seen in **Figure 9a**, it is evident that PAN nanofibers create a compact structure by scaffolding atop each other. Elemental distribution tests also confirm that PAN is a carbon polymer by detecting carbon via EDX analysis (**Figure 9b**).

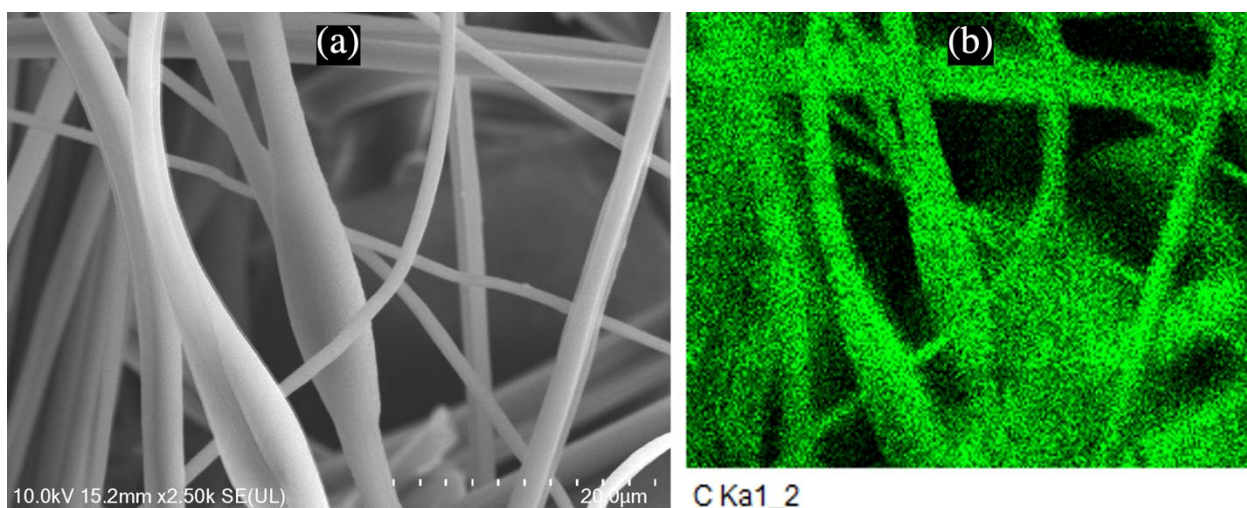


Figure 9. (a) SEM Image of Pure PAN Nanofibers (b) Elemental Distribution of Carbon in SEM Image of Pure PAN Nanofibers

SEM techniques were utilized to further investigate the presence of AgNPs and CuNPs on PAN nanofibers. As seen in **Figure 10** and **Figure 11**, it can be observed that AgNPs and CuNPs are scattered and distributed atop PAN-AgNP and PAN-CuNP nanofibers, respectively. **Table 1**, **Figure A3**, and **Figure A4** also indicate that higher elemental weight concentrations of silver and copper were respectively found on PAN nanofibers synthesized from higher wt.% concentrations of AgNO_3 and CuSO_4 .

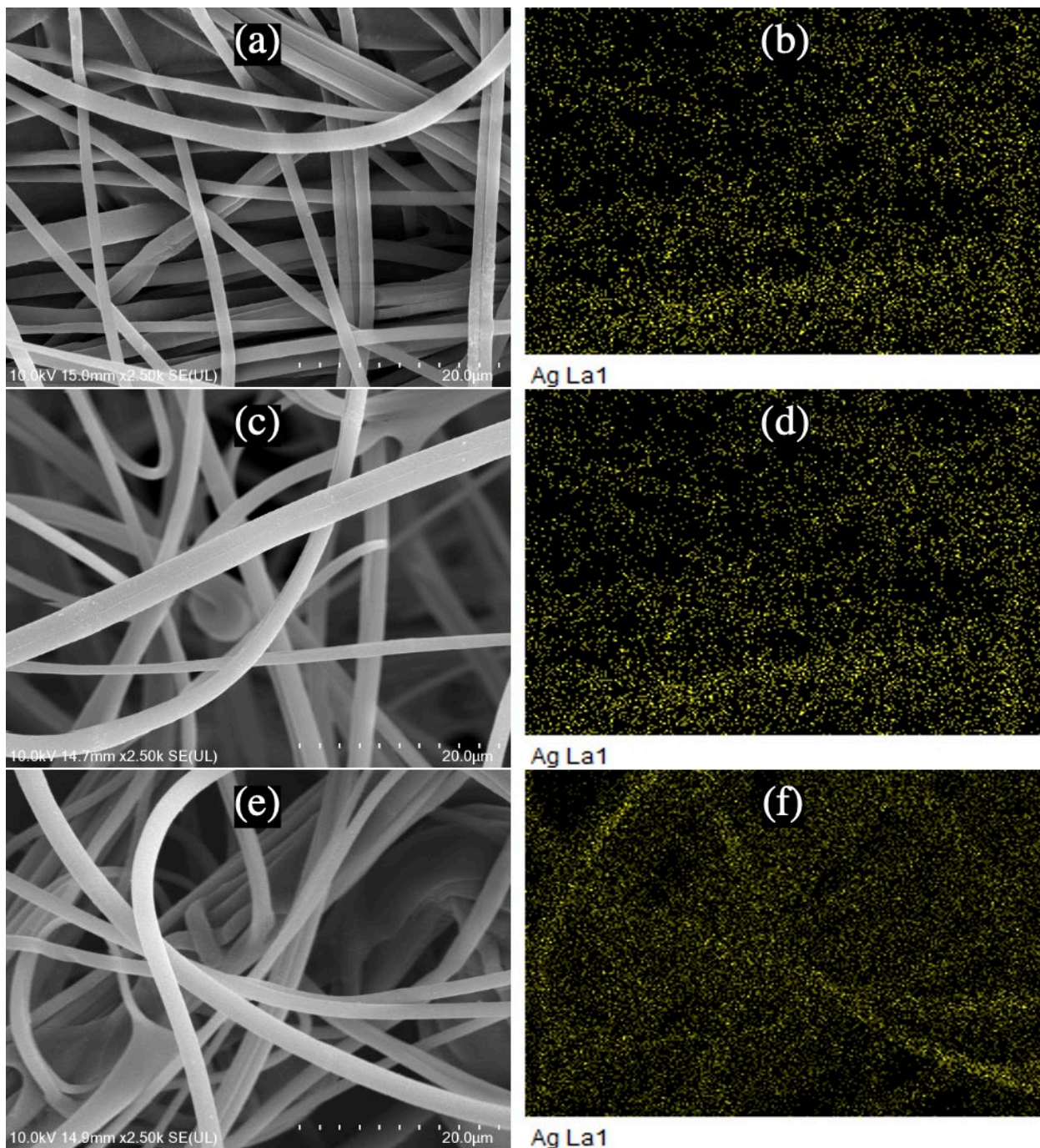


Figure 10. (a) SEM Image of 5% PAN-AgNP Nanofibers **(b)** Elemental Distribution of Silver in SEM Image of 5% PAN-AgNP Nanofibers **(c)** SEM Image of 10% PAN-AgNP Nanofibers **(d)** Elemental Distribution of Silver in SEM Image of 10% PAN-AgNP Nanofibers **(e)** SEM Image of 15% PAN-AgNP Nanofibers **(f)** Elemental Distribution of Silver in SEM Image of 15% PAN-AgNP Nanofibers

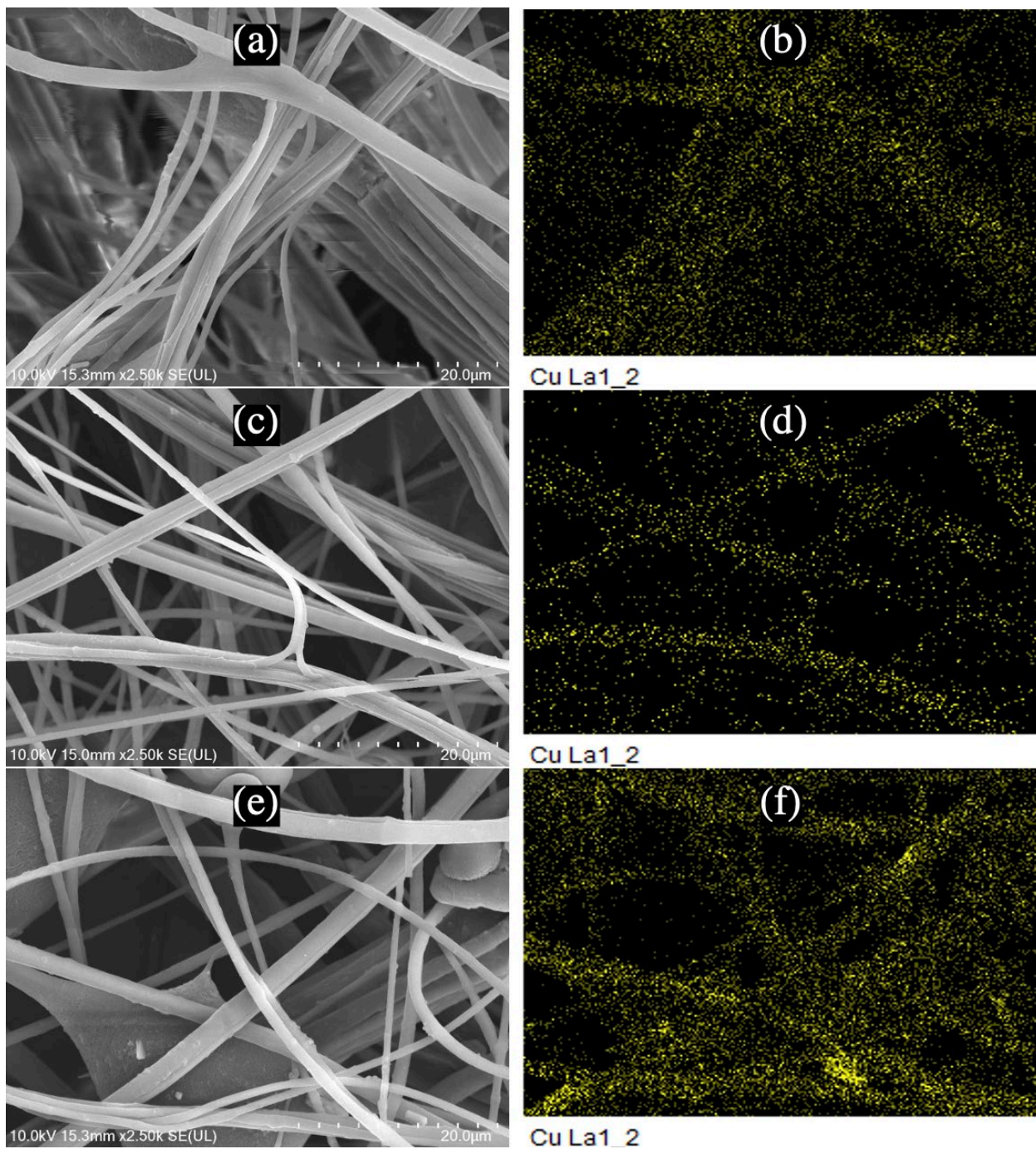


Figure 11. (a) SEM Image of 5% PAN-CuNP Nanofibers (b) Elemental Distribution of Copper in SEM Image of 5% PAN-CuNP Nanofibers (c) SEM Image of 10% PAN-CuNP Nanofibers (d) Elemental Distribution of Copper in SEM Image of 10% PAN-CuNP Nanofibers (e) SEM Image of 15% PAN-CuNP Nanofibers (f) Elemental Distribution of Copper in SEM Image of 15% PAN-CuNP Nanofibers

Table 1. Average Silver and Copper Elemental Weight Concentration for PAN-AgNP and PAN-CuNP Nanofibers Synthesized from Different wt.% Concentrations of AgNO₃ and CuSO₄

Sample Classification	Average Elemental Weight Concentration (%)	
	PAN-AgNP Nanofiber	PAN-CuNP Nanofiber
5% wt.% Concentration	4.12	3.05
10% wt.% Concentration	7.85	3.69
15% wt.% Concentration	10.08	4.36

6.3. Characterization of AgNP and CuNP Size with TEM and DLS

AgNPs and CuNPs found on PAN nanofibers were also characterized for their particle sizes using TEM analysis. Examples of this are shown in TEM images in **Figures 12a** and **13a**, which depict the TEM image of multiple AgNPs and CuNPs, respectively. Isolated, non-clustered AgNPs and CuNPs were observed to be scattered in PAN/DMF/AgNP and PAN/DMF/CuNP colloidal solutions and were measured for their size. AgNPs and CuNPs analyzed using TEM techniques had relatively spherical structures that varied in size and shape. The elemental distributions of silver (**Figure 12b**) and copper (**Figure 13b**) and their subsequent EDX Spectra (**Figure 14**, **Figure 15**) peaks also demonstrate that the particles imaged with the TEM were indeed AgNPs and CuNPs as high intensities of silver and copper were measured in regions that contained the particles.

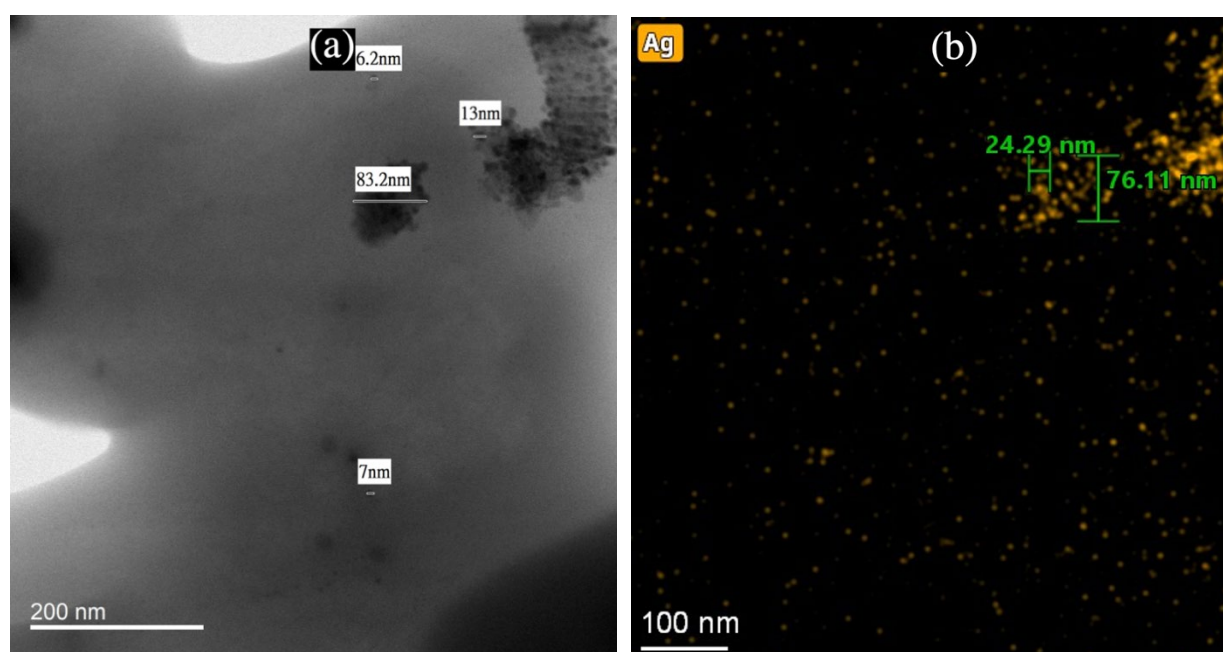


Figure 12. (a) TEM Image of AgNPs of Various Sizes in PAN/DMF/AgNP Colloidal Solution **(b)** Elemental Distribution of Silver in TEM Image of PAN/DMF/AgNP Colloidal Solution

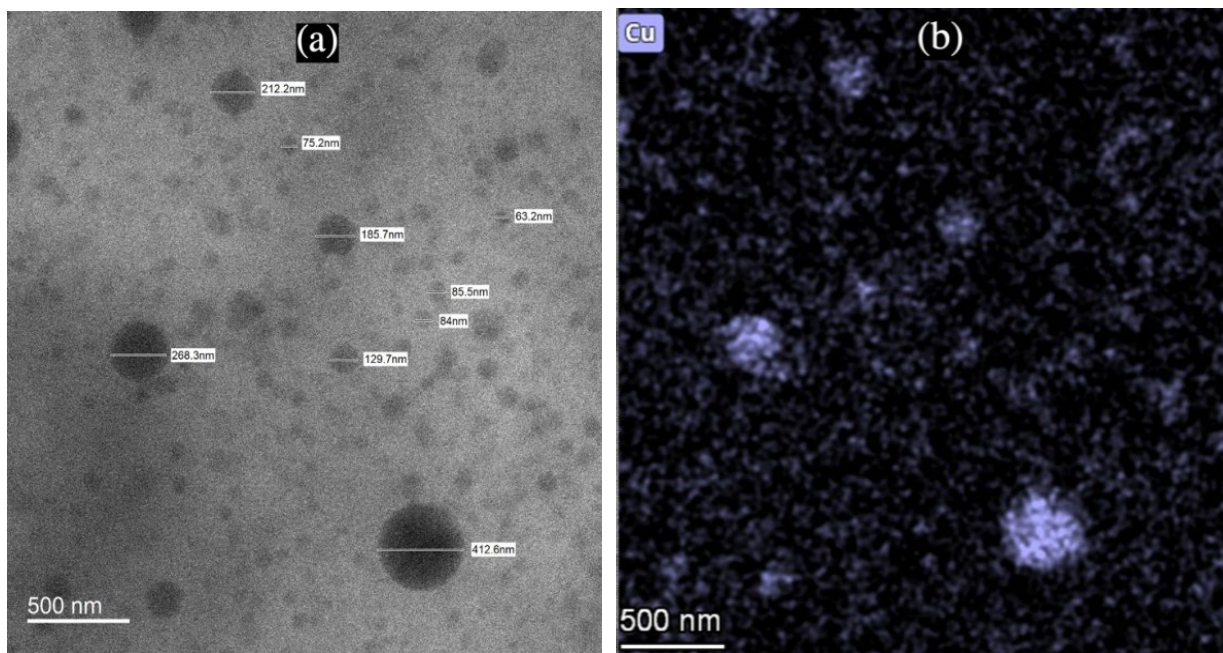


Figure 13. (a) TEM Image of CuNPs of Various Sizes in PAN/DMF/CuNP Colloidal Solution
(b) Elemental Distribution of Copper in TEM Image of PAN/DMF/CuNP Colloidal Solution

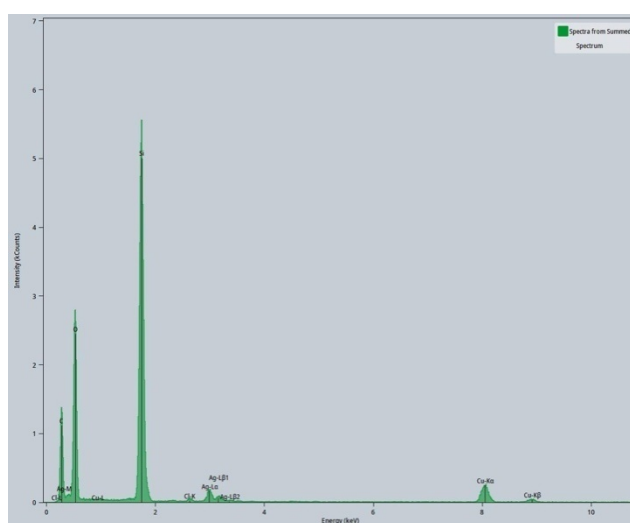


Figure 14. EDX Spectrum of PAN/DMF/AgNP Colloidal Solution

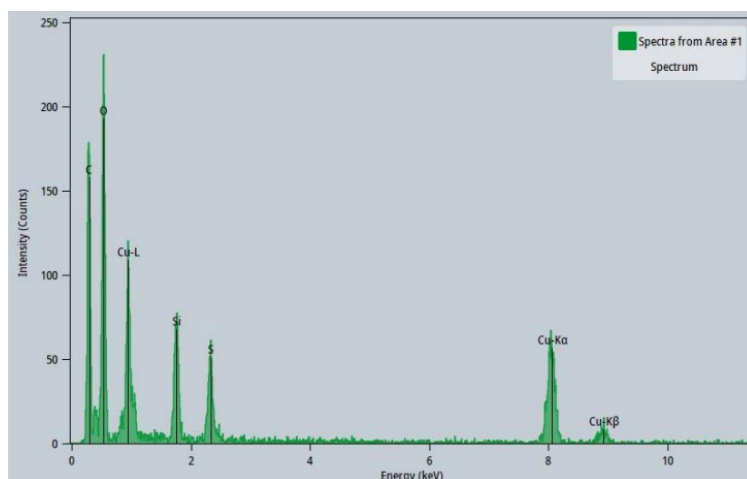


Figure 15. EDX Spectrum of PAN/DMF/CuNP Colloidal Solution

Dynamic Light Scattering was also used to examine the size distributions of AgNPs and CuNPs found in PAN/DMF/AgNP and PAN/DMF/CuNP colloidal solutions. Results from DLS further reinforced the AgNPs and CuNPs diameter measurements obtained using TEM techniques (**Figure 16**, **Figure 17**). Larger particle measurements could have been incidences of clusters of AgNPs or CuNPs being identified together as a singular particle.

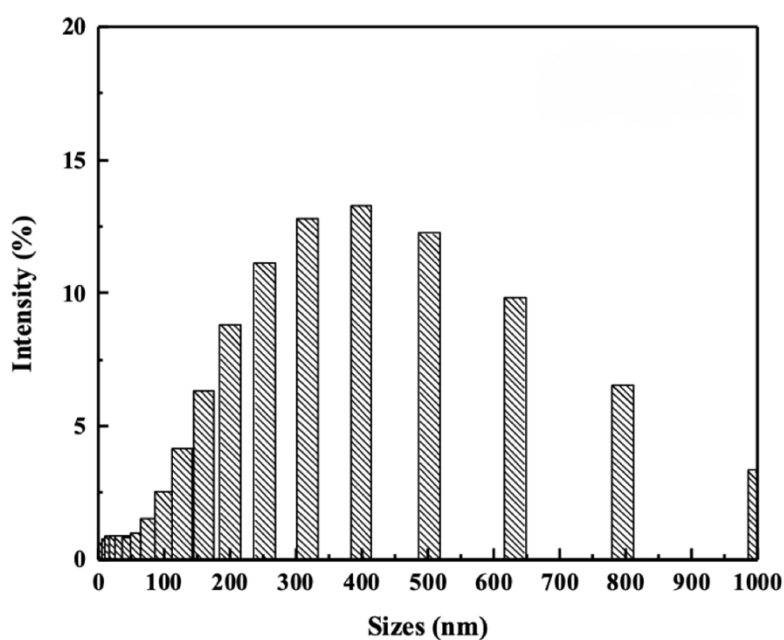


Figure 16. Dynamic Light Scattering Spectrum of 15% PAN/DMF/AgNP Colloidal Solution

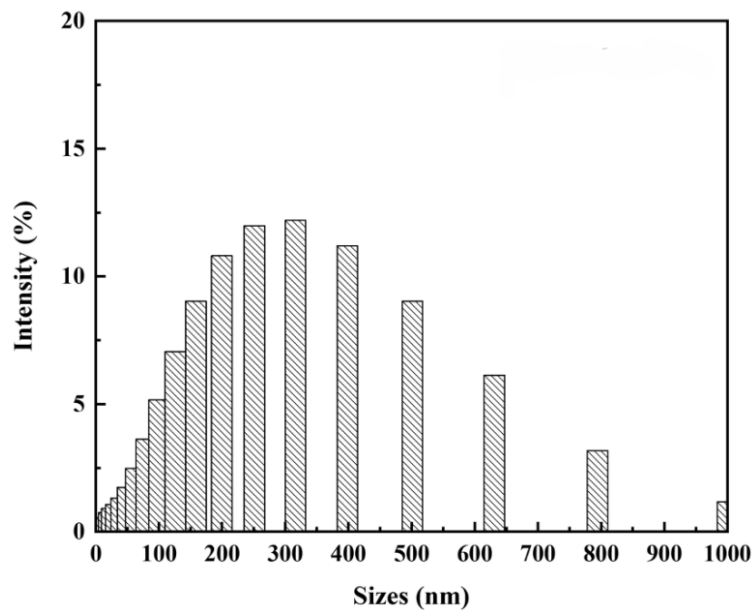


Figure 17. Dynamic Light Scattering Spectrum of 15% PAN/DMF/CuNP Colloidal Solution

6.4. Comparison of Preserved and New PAN-AgNP and PAN-CuNP Nanocomposites

As seen in **Figure 18a**, preserved PAN-AgNP nanofibers (as shown on the left) had a brown-black hue while new PAN-AgNP nanofibers were white. Similarly, as seen in **Figure 18b**, preserved PAN-CuNP nanofibers (as shown on the left) had a green hue while new PAN-CuNP nanofibers were white.

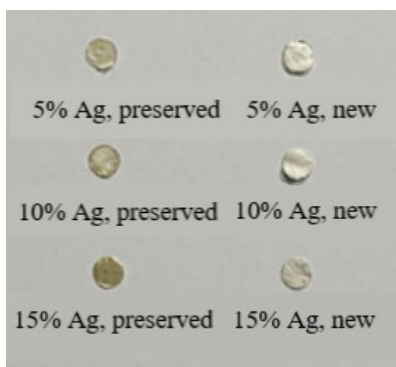


Figure 18a. Preserved and New PAN-AgNP Nanofibers

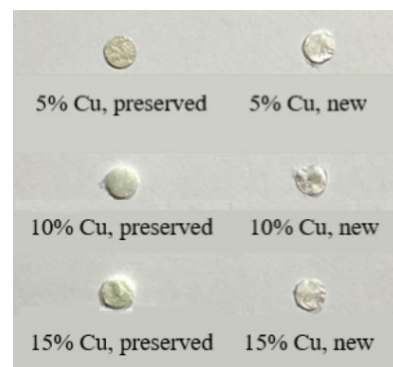


Figure 18b. Preserved and New PAN-CuNP Nanofibers

6.5. Antibacterial Efficiency Tests on *E. coli* and *L. crispatus*

E. coli and *L. crispatus* were used for PAN-AgNP and PAN-CuNP nanofiber antibacterial efficiency tests due to their ubiquitous nature and optimal growth kinetics. As BioSafety Level

1 (BSL-1) bacteria, both bacteria are also extremely accessible and prove to be safe options for antibacterial efficiency tests.

As seen in **Table 2** and **Table 3**, pure PAN nanofiber and copper foil disks do not have any antibacterial properties on *E. coli*. On the other hand, bulk silver foil disks demonstrated visible antibacterial activity. Moreover, PAN-AgNP and PAN-CuNP nanofibers synthesized from higher wt.% concentrations of AgNO₃ and CuSO₄ showed improved antibacterial efficiency on *E. coli* when compared to their bulk counterparts; increases in ZOI diameter measurements were also correlated to increased wt.% concentrations of AgNO₃ and CuSO₄. Silver nanocomposites and disks also proved to be more efficient antibacterial agents against *E. coli* compared to copper nanocomposites and disks.

Table 2. Antibacterial Efficiency of PAN-AgNP Nanofibers Synthesized from Different wt.% of AgNO₃ and Silver Foil Disks Against *E. coli*

Sample Classification	New		Preserved	
	Average ZOI Diameter (mm)	Standard Deviation	Average ZOI Diameter (mm)	Standard Deviation
Pure PAN Nanofiber	0	0	N/A	N/A
Silver Foil Disk	6.7	0.09	N/A	N/A
5% PAN-AgNP Nanofiber	7.3	0.22	7.0	0.19
10% PAN-AgNP Nanofiber	7.5	0.25	7.5	0.05
15% PAN-AgNP Nanofiber	8.2	0.16	7.5	0.12

Table 3. Antibacterial Efficiency of PAN-CuNP Nanofibers Synthesized from Different wt.% of CuSO₄ and Copper Foil Disks Against *E. coli*

Sample Classification	New		Preserved	
	Average ZOI Diameter (mm)	Standard Deviation	Average ZOI Diameter (mm)	Standard Deviation
Pure PAN Nanofiber	0	0	N/A	N/A
Copper Foil Disk	0	0	N/A	N/A
5% PAN-CuNP Nanofiber	6.7	0.17	6.7	0.09
10% PAN-CuNP Nanofiber	6.6	0.05	6.7	0.12
15% PAN-CuNP Nanofiber	6.9	0.09	6.8	0.17

PAN-AgNP and PAN-CuNP nanocomposites that were preserved for approximately 90 days generally demonstrated similar antibacterial activity against *E. coli* when compared to new nanocomposites; our experimental data showed that all but one of the differences in measured ZOI diameter between preserved and new samples against *E. coli* were not

statistically significant (**Figure 19**). **Figure 19c** indicates that new 15% PAN-AgNP nanocomposites performed better than their preserved counterparts, as their differences in measured ZOI diameter were statistically significant.

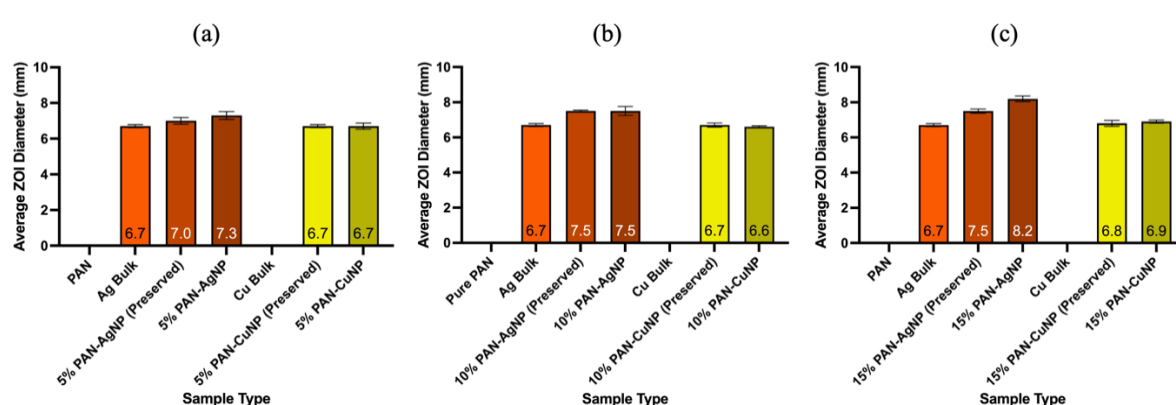


Figure 19. (a) Antibacterial Efficiency of 5% PAN-AgNP and 5% PAN-CuNP Nanofibers on *E. coli* (b) Antibacterial Efficiency of 10% PAN-AgNP and 10% PAN-CuNP Nanofibers on *E. coli* (c) Antibacterial Efficiency of 15% PAN-AgNP and 15% PAN-CuNP Nanofibers on *E. coli*

Similar to previous trials on *E. coli*, pure PAN nanofiber and bulk copper foil disks do not have any antibacterial properties against *L. crispatus*, while bulk silver foil disks demonstrated antibacterial activity (**Table 4**, **Table 5**). PAN-AgNP and PAN-CuNP nanofibers synthesized from higher wt.% concentrations of AgNO₃ and CuSO₄ yet again showed improved antibacterial efficiency on *L. crispatus* when compared to their bulk counterparts; increases in ZOI diameter measurements were also correlated to increased wt.% concentrations of AgNO₃ and CuSO₄. Silver nanocomposites and disks also proved to be more efficient antibacterial agents against *L. crispatus* compared to copper nanocomposites and disks.

Table 4. Antibacterial Efficiency of PAN-AgNP Nanofibers Synthesized from Different wt.% of AgNO₃ and Silver Foil Disks Against *L. crispatus*

Sample Classification	New		Preserved	
	Average ZOI Diameter (mm)	Standard Deviation	Average ZOI Diameter (mm)	Standard Deviation
Pure PAN Nanofiber	0	0	N/A	N/A
Silver Foil Disk	7.6	0.46	N/A	N/A
5% PAN-AgNP Nanofiber	11.5	0.17	9.8	0.34
10% PAN-AgNP Nanofiber	12.0	0.22	10.2	0.37
15% PAN-AgNP Nanofiber	13.4	0.05	10.4	0.42

Table 5. Antibacterial Efficiency of PAN-CuNP Nanofibers Synthesized from Different wt.% of CuSO₄ and Copper Foil Disks Against *L. crispatus*

Sample Classification	New		Preserved	
	Average ZOI Diameter (mm)	Standard Deviation	Average ZOI Diameter (mm)	Standard Deviation
Pure PAN Nanofiber	0	0	N/A	N/A
Copper Foil Disk	0	0	N/A	N/A
5% PAN-CuNP Nanofiber	7.6	0.17	6.7	0.21
10% PAN-CuNP Nanofiber	8.2	0.12	6.7	0.04
15% PAN-CuNP Nanofiber	8.5	0.09	7.2	0.16

New PAN-AgNP and PAN-CuNP nanocomposites had better antibacterial efficiency against *L. crispatus* when compared to nanocomposites that were preserved for approximately 90 days. Our experimental data revealed that all of the differences in measured ZOI diameter between preserved and new samples against *L. crispatus* were statistically significant, as error bars do not overlap (**Figure 20**). When comparing **Figure 19** to **Figure 20**, it can be observed that all disks and nanocomposites had higher antibacterial efficiency against *L. crispatus* compared to *E. coli*.

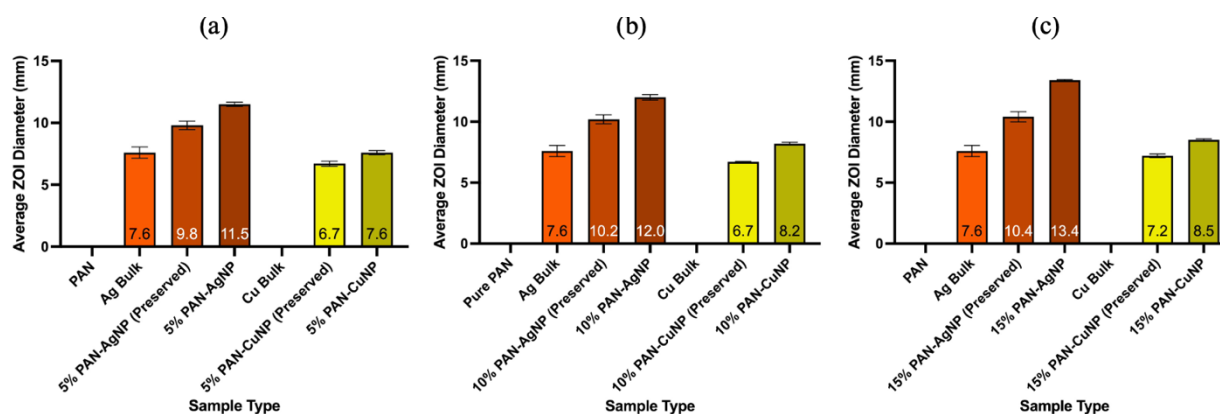


Figure 20. (a) Antibacterial Efficiency of 5% PAN-AgNP and 5% PAN-CuNP Nanofibers on *L. crispatus* (b) Antibacterial Efficiency of 10% PAN-AgNP and 10% PAN-CuNP Nanofibers on *L. crispatus* (c) Antibacterial Efficiency of 15% PAN-AgNP and 15% PAN-CuNP Nanofibers on *L. crispatus*

7. Discussion

7.1. Colloidal Synthesis and Polymer Characterization

This study successfully created a novel antibacterial nanocomposite by utilizing chemical reduction and electrospinning methodologies. DMF, while conventionally used as an organic

solvent in chemistry experiments, plays three crucial roles in our research – it is a prominent electrospinning solvent, a potent metal salt reducing agent, and also acts as a metal nanoparticle protectant [20]. Because of its dielectric, low vapor pressure nature, DMF serves as a great electrospinning base as charged DMF colloidal solutions will be able to overcome their own surface tension before evaporating and subsequently decreasing the diameter of the Taylor Cone [22]. By having high oxidative potential due to its possession of an aldehyde group, DMF also can chemically reduce metal ions found in metal salts to their atomic forms, essentially synthesizing metal NPs during the process. DMF also prevents the agglomeration of NPs by acting as a protectant in surfactant free colloidal nanoparticle solution synthesis [24].

Furthermore, PAN-CuNP nanofibers retain their reductive state after approximately 90 days of preservation. As seen in our XPS tests for new PAN-CuNP nanocomposites (**Figure A1, Table A1**) and preserved PAN-CuNP nanocomposites (**Figure A2, Table A2**), new and preserved PAN-CuNP nanocomposites show similar atomic weight concentration compositions for both Cu₂O/Cu-Cu and CuO detections.

Therefore, as seen from AFM, SEM, TEM and DLS tests, metal NPs have successfully formed in both PAN/DMF solutions and electrospun PAN nanofibers. SEM and TEM EDX Analysis spectra further confirm the presence of AgNPs and CuNPs in both PAN/DMF solutions and PAN nanofibers. These results show that our method of synthesis via chemical reduction and electrospinning proves to be successful when it comes to creating metal nanoparticle carbon polymer nanocomposites.

7.2. Evaluation of Nanocomposite Antibacterial Efficiency

Our data from ZOI tests indicate that all nanocomposite disks for both silver and copper based materials outperformed their bulk counterparts against both *E. coli* and *L. crispatus* – in fact, bulk copper disks had no antibacterial activity at all. Hence, this reveals that once silver and copper have been synthesized into nanomaterials, they become potent antimicrobials; due to nanomaterials having increased surface area-to-volume ratio, AgNPs and CuNPs can bind to bacteria cells and disrupt their organic and chemical processes, eventually causing cellular death. Pure PAN polymers do not possess any antimicrobial activity; however, they serve as vessels for metal NPs, allowing them to avoid agglomeration and interact with and eliminate more pathogens.

It is also evident that silver is a better antimicrobial agent than copper, as bulk Ag disks demonstrated a certain degree of antimicrobial activity against both test bacteria while all bulk Cu disks failed to create any zone of inhibition. Moreover, PAN-AgNP nanocomposite disks outperformed their respective PAN-CuNP nanocomposite disks of the same concentration in terms of antibacterial efficiency for both *E. coli* and *L. crispatus*. This is because AgNPs have

better diffusivity when compared to CuNPs – it is easier for AgNPs to permeate amongst bacteria colonies and in turn eliminate more bacteria and create a larger zone of inhibition [25].

PAN-AgNP and PAN-CuNP nanocomposites preserved at room temperature for approximately 90 days prior to incubation also maintained antibacterial efficiency against both *E. coli* and *L. crispatus*.

Both PAN-AgNP and PAN-CuNP nanocomposites had more antibacterial efficiency against *L. crispatus* compared to *E. coli*. We suspect that this discrepancy occurred because of the different gram classifications for *L. crispatus* and *E. coli*; *L. crispatus* is a gram-positive bacteria while *E. coli* is a gram-negative bacteria. Differences in nanocomposite antibacterial efficiency against gram-positive and gram-negative bacteria possibly originated from the presence of an additional lipopolysaccharide-based outer membrane in gram-negative bacteria. Lipopolysaccharide plays a crucial role as a barrier that prevents the passive diffusion of hydrophobic substances, such as antibiotics and detergent, into the bacteria cell [26]. On the other hand, Gram-positive bacteria do not have an outer membrane; instead, they possess multiple layers of densely packed and ordered peptidoglycan chains in their cell wall [27].

8. Conclusion

AFM, SEM, TEM, EDX, and DLS tests successfully confirmed and signified the formation of AgNPs and CuNPs on PAN nanofibers.

The formation of reduced AgNPs and CuNPs scaffolded upon PAN polymers can decrease nanoparticle aggregation and increase antibacterial efficiency against *E. coli* and *L. crispatus* due to a heightened surface area-to-volume ratio. We reveal that PAN-AgNP and PAN-CuNP nanocomposites have more antibacterial efficiency when compared to their bulk counterparts. Furthermore, nanofibers synthesized from higher wt.% concentrations of AgNO₃ and CuSO₄ demonstrated heightened antibacterial efficiency against *E. coli* and *L. crispatus*. Our data also indicates that AgNPs are better antibacterial agents as compared to CuNPs and that samples preserved approximately 90 days prior to incubation generally maintain their antibacterial efficiency. Although PAN-AgNP nanocomposites are more effective than PAN-CuNP nanocomposites against bacteria, copper is relatively cheaper than silver.

Conventional antibiotics are usually more expensive and stored under more specific conditions compared to carbon nanofibers coated with AgNPs or CuNPs, meaning that PAN-AgNP and PAN-CuNP nanofibers can be used as an effective alternative antibacterial material that is also more cost-effective and easier to store in certain industries or fields of study [28,29].

Thus, PAN-AgNP and PAN-CuNP nanocomposites could also be engineered or implemented onto high contact surfaces such as masks, pads, gloves, carpets, or surgical equipment.

9. Future Works

Our current study on the antimicrobial activity of PAN-AgNP and PAN-CuNP nanocomposites against *E. coli* and *L. crispatus* would serve as a preliminary test for other serial antimicrobial experiments.

We would like to create new NPs based PAN nanocomposites with metals like zinc (Zn) and iron (Fe). While neither element is known to have antimicrobial properties in their bulk forms, our data for bulk copper disks and PAN-CuNP nanocomposites demonstrate that materials synthesized to the nanoscale could eliminate bacteria because of their increased surface area-to-volume ratio. Furthermore, like copper, both zinc and iron are trace elements in the human body, meaning that they are safer for human use as opposed to other elements.

Our qualifications for access to a BSL-2 laboratory has also been granted via the successful completion of a Lab Biosafety Manual and Biosecurity Guidance Training Course in Fu Jen Catholic University (**Figure A11**). We have already started conducting tests on various BioSafety Level 2 (BSL-2) pathogens (which cannot be used for experimentation at the Macronix High School Science Awards), including *Staphylococcus aureus*, *Klebsiella pneumoniae*, and more. Conducting tests on a wider variety of antibiotic resistant pathogens will allow this study to expand its impact by targeting a larger scope of refractory infective diseases.

Last but not least, we have also began experimentation on *Candida albicans* (*C. albicans*) and will compare our new experimental results to that of *L. crispatus*. The ratio between these two bacteria directly influences the possibility of contraction of female genitourinary diseases. Therefore, if these nanocomposites demonstrate more antibacterial activity against *C. albicans* than *L. crispatus*, they could be made into coatings for pads or pantyliners in order to reduce the risk for genitourinary infection.

10. References

1. Yang, S.; Hua, M.; Liu, X.; Du, C.; Pu, L.; Xiang, P.; Wang, L.; Liu, J. Bacterial and fungal co-infections among COVID-19 patients in intensive care unit. *Microbes Infect.* **2021**, *23*, 104806.
2. Liu, L.; Li, Y.; Nielsen, P.V.; Wei, J.; Jensen, R.L. Short-range airborne transmission of expiratory droplets between two people. *Indoor Air* **2017**, *27*, 452–462.
3. Guzman, M.I. An overview of the effect of bioaerosol size in coronavirus disease 2019 transmission. *Int. J. Health Plan. Manag.* **2021**, *36*, 257–266
4. Zhitnitsky, D.; Rose, J.; Lewinson, O. The highly synergistic, broad spectrum, antibacterial activity of organic acids and transition metals. *Sci. Rep.* **2017**, *7*, 1–13.
5. Rai; Mahendra; Alka Y.; Aniket Gade. Silver nanoparticles as a new generation of antimicrobials. *Biotechnol. Adv.* **2009**, *1*, 76-83.
6. Vincent, M.; Hartemann, P.; Engels-Deutsch, M. Antimicrobial applications of copper. *Int. J. Hyg. Environ. Health* **2016**, *219*, 585–591.
7. Vincent, M.; Duval, R.E.; Hartemann, P.; Engels-Deutsch, M. Contact killing and antimicrobial properties of copper. *J. Appl. Microbiol.* **2018**, *124*, 1032–1046.
8. Hoseinzadeh, E.; Makhdoumi P.; Taha P.; Hossini H.; Stelling J.; Kamal M.A. A review on nano-antimicrobials: metal nanoparticles, methods and mechanisms. *Curr. Drug Metab.* **2017**, *18(2)*, 120-128
9. Chatterjee, A.K.; Chakraborty, R.; Basu, T. Mechanism of antibacterial activity of copper nanoparticles. *Nanotechnology* **2014**, *25*, 135101.
10. Konieczny, J.; Rdzawski, Z. Antibacterial properties of copper and its alloys. *Arch. Mater. Sci. Eng.* **2012**, *56*, 53–60.
11. Samoilova, N.; Krayukhina, M.; Naumkin, A.; Anuchina, N.; Popov, D. Silver nanoparticles doped with silver cations and stabilized with maleic acid copolymers: specific structure and antimicrobial properties. *New J. Chem.* **2021**, *45*, 14513–14521
12. Khodashenas, B.; Ghorbani, H.R. Synthesis of silver nanoparticles with different shapes. *Arab. J. Chem.* **2019**, *12*, 1823–1838.
13. Lemraski, E.G.; Jahangirian, H.; Dashti, M.; Khajehali, E.; Sharafinia, S.; Rafiee-Moghaddam, R.; Webster, T.J. Antimicrobial double-layer wound dressing based on chitosan/polyvinyl alcohol/copper: in vitro and in vivo assessment. *Int. J. Nanomed* **2021**, *16*, 223.
14. Persano, L.; Camposeo, A.; Tekmen, C.; Pisignano, D. Industrial upscaling of electrospinning and applications of polymer nanofibers: a review. *Macromol. Mater. Eng.* **2013**, *298*, 504–520.
15. Xu, J.; Feng, X.; Chen, P.; Gao, C. Development of an antibacterial copper (II)-chelated polyacrylonitrile ultrafiltration membrane. *J. Membr. Sci.* **2012**, *413*, 62–69.

16. Yusof, N.; Ismail, A. Post spinning and pyrolysis processes of polyacrylonitrile (PAN)-based carbon fiber and activated carbon fiber: A review. *J. Anal. Appl. Pyrolysis*. **2012**, 93, 1–13.
17. Palza, H. Antimicrobial polymers with metal nanoparticles. *Int. J. Mol. Sci.* **2015**, 16, 2099–2116.
18. Claudel, M.; Schwarte, J.V.; Fromm, K.M. New antimicrobial strategies based on metal complexes. *Chemistry* **2020**, 2, 849–899.
19. Bashir, Z. A critical review of the stabilisation of polyacrylonitrile. *Carbon* **1991**, 29, 1081–1090.
20. Pastoriza-Santos, I.; Liz-Marzán, L.M. N, N-Dimethylformamide as a reaction medium for metal nanoparticle synthesis. *Adv. Funct. Mater.* **2009**, 19, 679–688.
21. Rodrigues; Thenner S.; Ming Z.; Yang T.-H.; Kyle D. Gilroy; Anderson G. S.; Pedro HC C.; Xia Y. Synthesis of colloidal metal nanocrystals: A comprehensive review on the reductants. *Chem. Eur. J.* **2018**, 16944-16963.
22. Du; Lei; Xu H.; Zhang Y.; Zou F. Electrospinning of polycaprolatone nanofibers with DMF additive: The effect of solution proprieties on jet perturbation and fiber morphologies. *Fibers Polym.* **2016**, 17, 751-759.
23. Chen, J. C.; I. R. Harrison. Modification of polyacrylonitrile (PAN) carbon fiber precursor via post-spinning plasticization and stretching in dimethyl formamide (DMF). *Carbon* **2002**, 25-45
24. Nagata, T.; Obora Y. N, N-dimethylformamide-protected single-sized metal nanoparticles and their use as catalysts for organic transformations. *ACS omega* **2019**, 1, 98-103.
25. Cunha, F. A.; Maia, K. R.; Mallman, E. J. J. Silver nanoparticles-disk diffusion test against *Escherichia coli* isolates. *Rev. Inst. Med. Trop. Sao Paulo* **2016**, 58, 73
26. Zhang, G. E.; Timothy C. M. ; Daniel K. On the essentiality of lipopolysaccharide to Gram-negative bacteria. *Curr. Opin. Microbiol.* **2013**, 6, 779-785.
27. Kim, S. J.; James C.; Manmilan S. Peptidoglycan architecture of Gram-positive bacteria by solid-state NMR. *Biochim. Biophys. Acta - Biomembr.* **2015**, 1, 350-362.
28. Filippini, M.; Masiero, G.; Moschetti, K. Regional consumption of antibiotics: a demand system approach. *Econ. Model* **2009**, 26, 1389–1397.
29. Kumru, O.S.; Joshi, S.B.; Smith, D.E.; Middaugh, C.R.; Prusik, T.; Volkin, D.B. Vaccine instability in the cold chain: mechanisms, analysis and formulation strategies. *Biologicals* **2014**, 42, 237–259.

Appendix

X-ray Photoelectron Spectroscopy (XPS) Tests

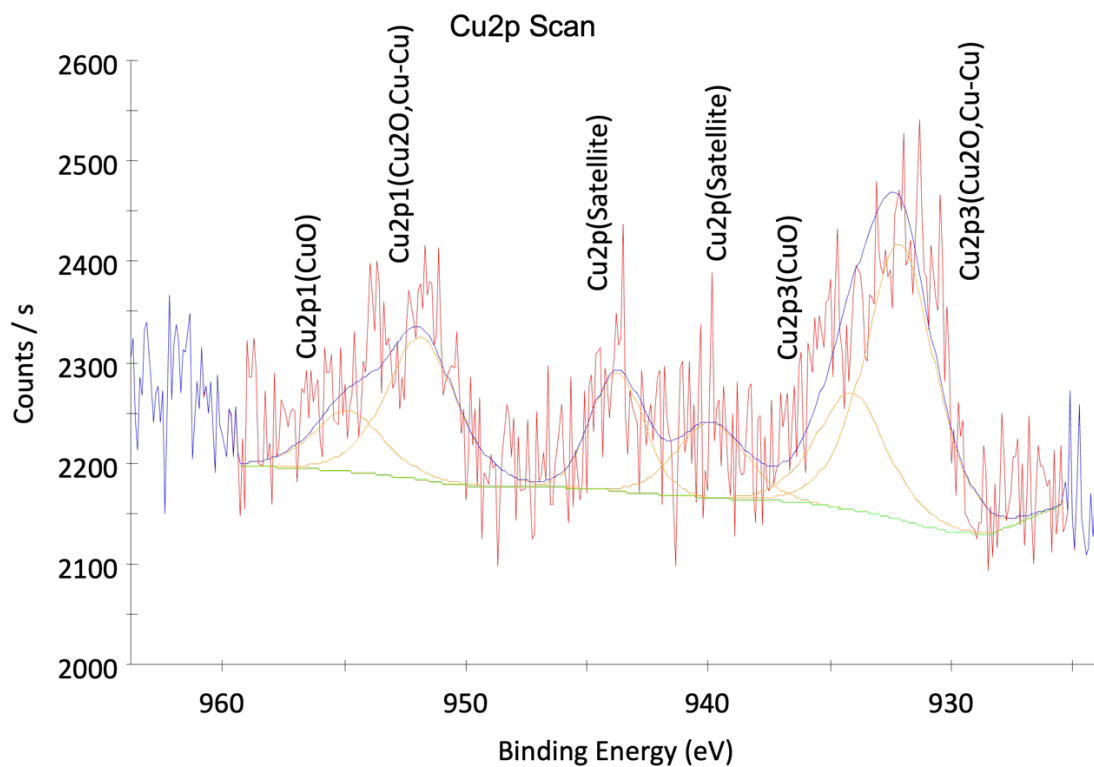


Figure A1. Cu2p XPS Core-Level Spectra of 15% PAN-CuNP Nanofiber Sample

Table A1. Cu2p XPS Atomic Weight Quantification of 15% PAN-CuNP Nanofiber Sample

XPS Detection Name	Atomic Weight Concentration (%)
Cu2p3 (Cu ₂ O, Cu-Cu)	70.1
Cu2p3 (CuO)	29.9

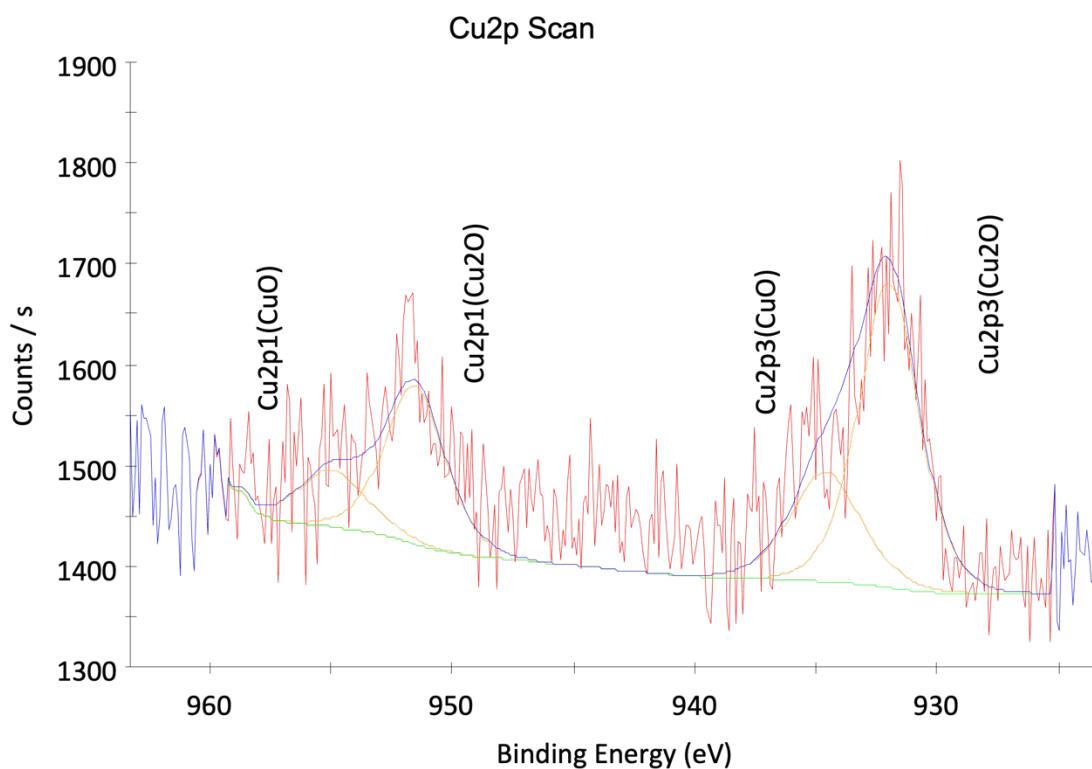


Figure A2. Cu2p XPS Core-Level Spectra of Preserved 15% PAN-CuNP Nanofiber Sample

Table A2. Cu2p XPS Atomic Weight Quantification of Preserved 15% PAN-CuNP Nanofiber Sample

XPS Detection Name	Atomic Weight Concentration (%)
Cu2p3 (Cu₂O, Cu-Cu)	70.6
Cu2p3 (CuO)	29.4

SU8220 SEM Energy Dispersive X-ray (EDX) Analysis

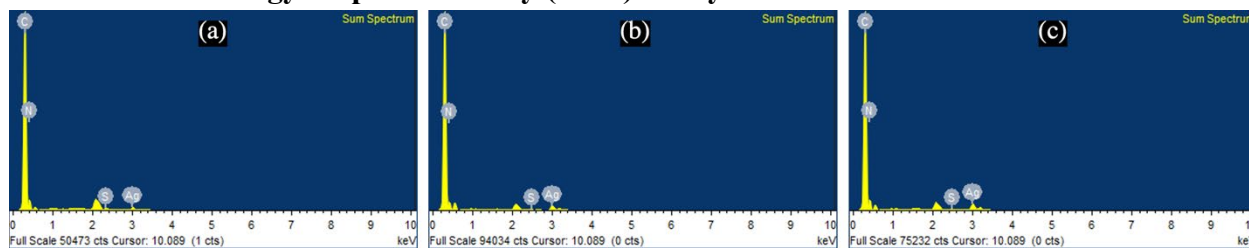


Figure A3. SEM EDX Spectrum of (a) 5% PAN-AgNP Nanofiber (b) 10% PAN-AgNP Nanofiber and (c) 15% PAN-AgNP Nanofiber

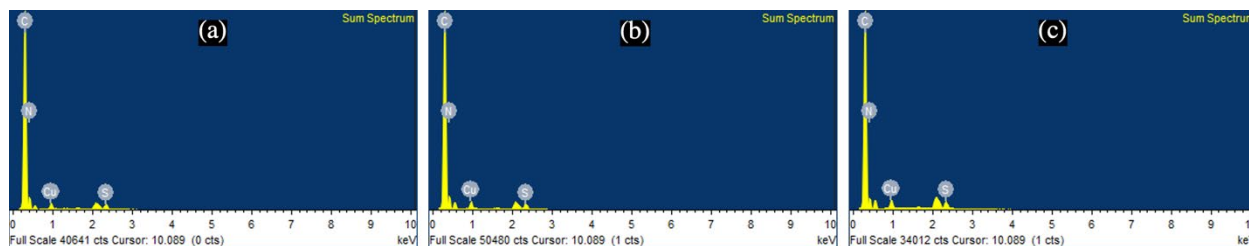


Figure A4. SEM EDX Spectrum of (a) 5% PAN-CuNP Nanofiber (b) 10% PAN-CuNP Nanofiber and (c) 15% PAN-CuNP Nanofiber

Phenom ProX G6 Desktop SEM Elemental Distribution/EDX Analysis

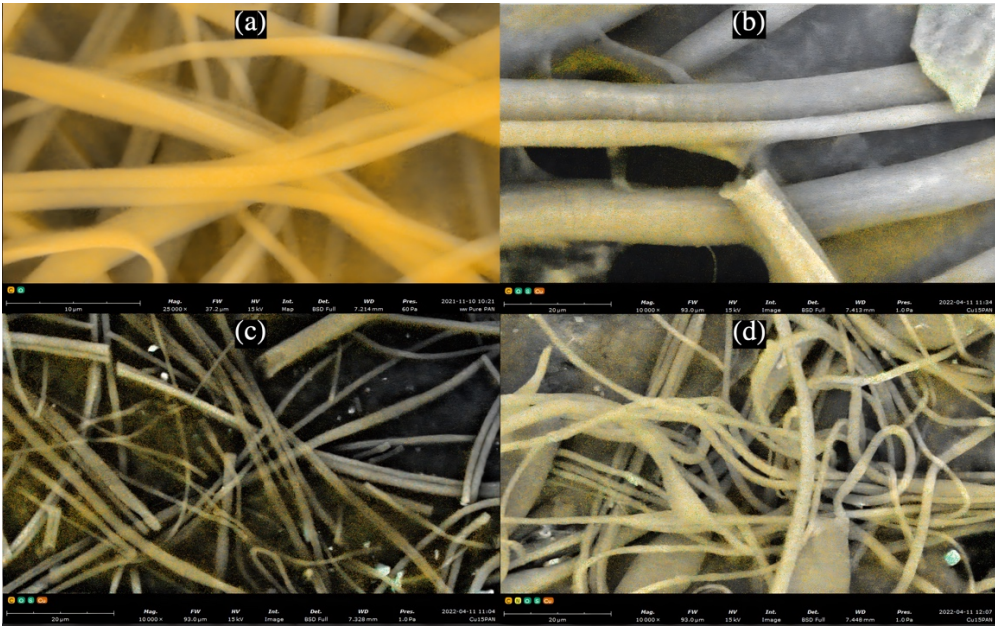


Figure A5. Phenom ProX G6 Desktop SEM (a) Elemental Distribution of Pure PAN Nanofibers (b) Elemental Distribution of 5% PAN-CuNP Nanofibers (c) Elemental Distribution of 10% PAN-CuNP Nanofibers (d) Elemental Distribution of 15% PAN-CuNP Nanofibers

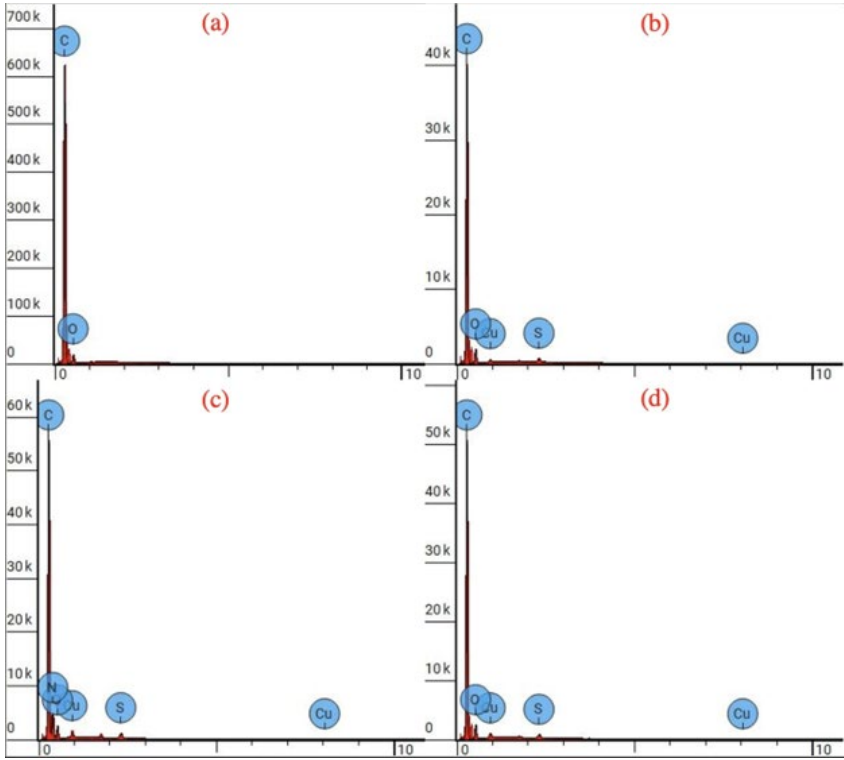
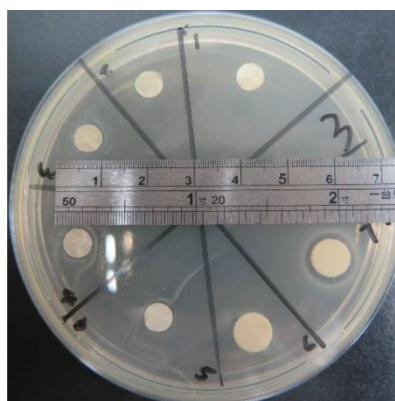
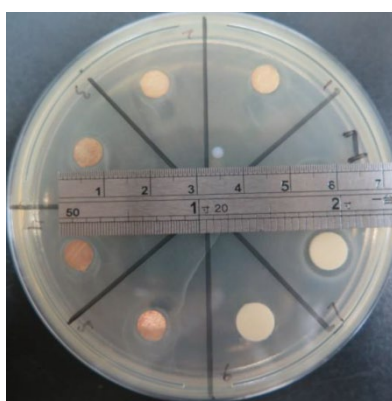


Figure A6. Phenom ProX G6 Desktop SEM (a) EDX Spectra of Pure PAN Nanofibers (b) EDX Spectra of 5% PAN-CuNP Nanofibers (c) EDX Spectra of 10% PAN-CuNP Nanofibers (d) EDX Spectra of 15% PAN-CuNP Nanofibers

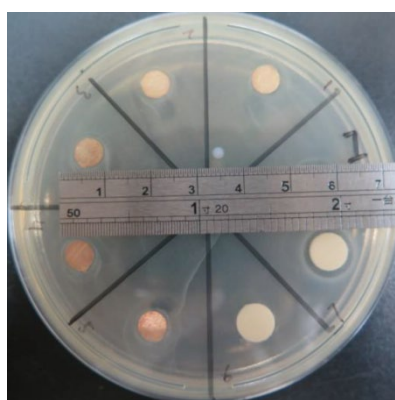
Nanocomposite Disk ZOI Test Photos for *E. coli* and *L. crispatus*



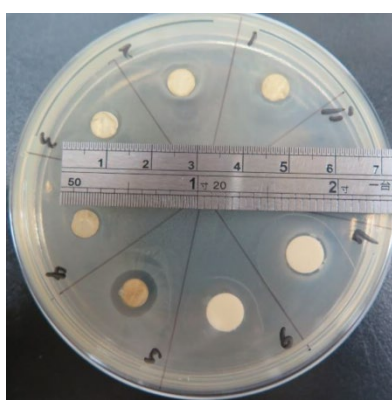
PAN



Ag bulk



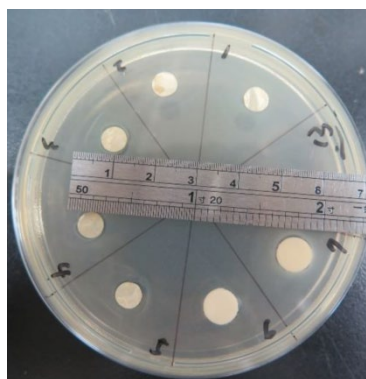
Preserved 5% Ag



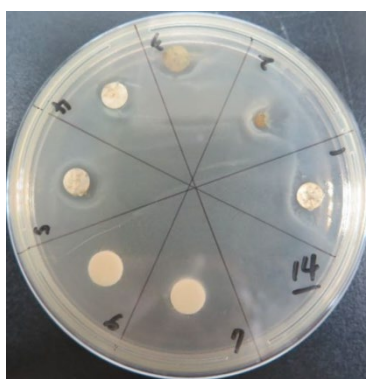
Preserved 10% Ag



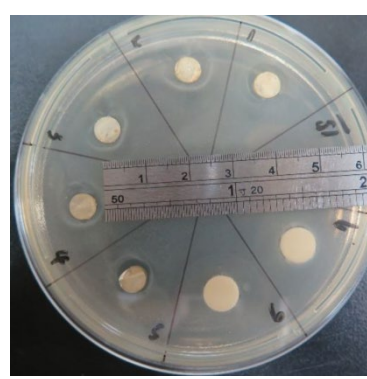
Preserved 15% Ag



New 5% Ag

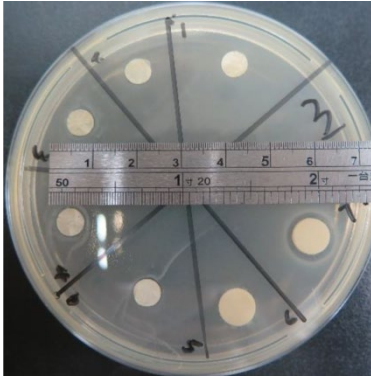


New 10% Ag

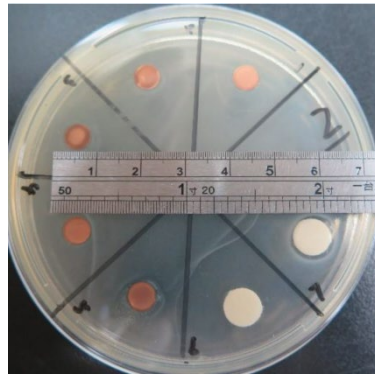


New 15% Ag

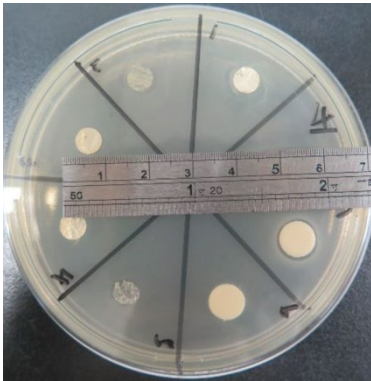
Figure A7. Ag Sample ZOI Tests on *E. coli*



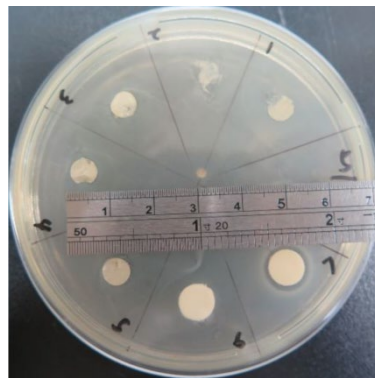
PAN



Cu bulk



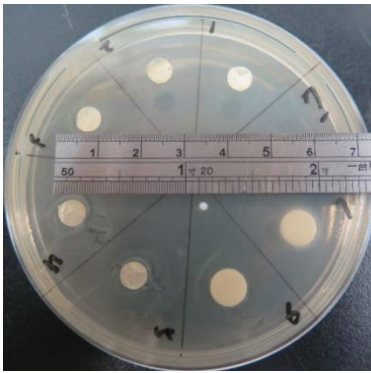
Preserved 5% Cu



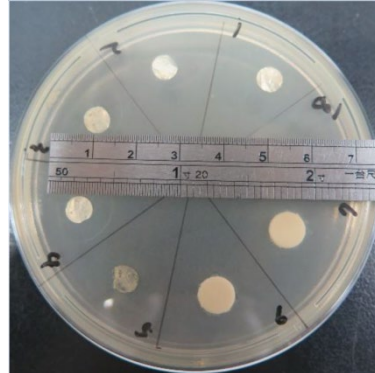
Preserved 10% Cu



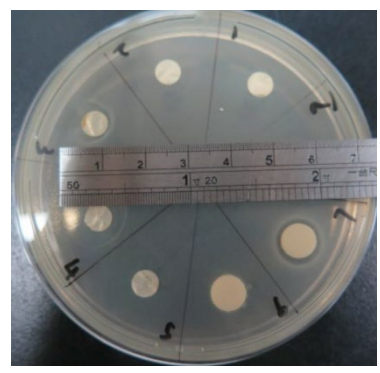
Preserved 15% Cu



New 5% Cu



New 10% Cu



New 15% Cu

Figure A8. Cu Sample ZOI Tests on *E. coli*



PAN



Ag bulk



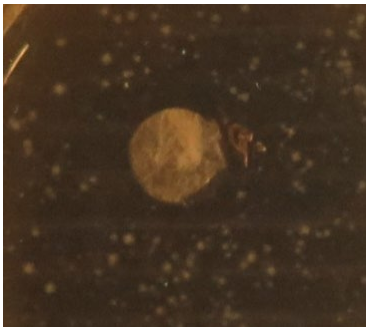
Preserved 5% Ag



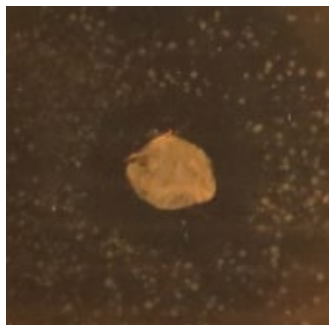
Preserved 10% Ag



Preserved 15% Ag



New 5% Ag



New 10% Ag



New 15% Ag

Figure A9. Ag Sample ZOI Tests on *L. crispatus*



PAN



Cu bulk



Preserved 5% Cu



Preserved 10% Cu



Preserved 15% Cu



New 5% Cu



New 10% Cu



New 15% Cu

Figure A10. Cu Sample ZOI Tests on *L. crispatus*



Figure A11. Fu Jen Catholic University Qualification Certificate for the 2021 Lab Biosafety Manual and Biosecurity Guidance Training Course